UPTEC X 01 047
NOV 2001

ISSN 1401-2138

FREDRIK ANDERSSON

Building a theoretical model describing capillary phenomena in microchannels in a plastic CD

Master’s degree project

Molecular Biotechnology Programme
Uppsala University School of Engineering

UPTEC X 01 047	**Date of issue 2001-11**

Author

Fredrik Andersson

Title (English)

Building a theoretical model describing capillary phenomena in microchannels in a plastic CD

Title (Swedish)

Abstract

Gyros AB develops a technology platform for miniaturisation of biomedical and biochemical applications. The base for this technology is a plastic CD with microstructures, where solutions move in a controlled way due to capillarity and centrifugal forces. In this work a theoretical model describing capillary phenomena in microchannels is proposed and examined. Such a model would be a valuable tool when designing new microstructures. Several different experiments were made in order to compare the model to measurements. The proposed model describes (quasi-) stationary situations fairly well, but fails to properly describe dynamic ones.

Keywords

Microfluidics, capillarity, imbibition, contact angle, Gyros AB.

Supervisors

Anders Hedström, Gyros AB

Examiner

Helene Dérand, Gyros AB

Project name	Sponsors
Language **English**	Security
ISSN 1401-2138	Classification
Supplementary bibliographical information	Pages **39**

Biology Education Centre Biomedical Center Husargatan 3 Uppsala
Box 592 S-75124 Uppsala Tel +46 (0)18 4710000 Fax +46 (0)18 555217

Building a Theoretical Model Describing Capillary Phenomena in Microchannels in a Plastic CD.

Fredrik Andersson

Sammanfattning

Gyros AB utvecklar en apparat som kommer att kunna utföra biologiska och medicinska analyser i mycket mindre skala än vad som görs idag. Basen för deras analyssystem är en plastskiva som ser ut som en CD-skiva. På skivan finns system av små kanaler i vilka analyserna görs. Skivan blir som ett laboratorium i miniatyr.

Precis som i ett vanligt laboratorium blandar man olika vätskor och lösningar för att göra sina analyser. I skivan flyttas vätskorna genom att styra dem så att de flyttar sig av sig själv (på grund av kapillärkrafter) eller genom att tvinga dem att flytta sig genom att spinna skivan snabbt (centrifugalkrafter).

Mitt examensarbete har gått ut på att försöka förutse hur kapillärkrafterna och centrifugalkrafterna får vätskan att röra sig. Jag har tagit fram formler som kan användas för att beräkna hur snabbt en vätska rör sig i en kanal, beroende på hur kanalen ser ut, eller som säger när vätskan börjar röra sig om man exempelvis spinner skivan.

Formlerna fungerar bra om de används för att räkna på något som händer innan vätskan börjar röra på sig. Om de användes för att beräkna hur snabbt en vätska rör sig, fås alldeles för höga hastigheter.

Building a Theoretical Model Describing Capillary Phenomena in Microchannels in a Plastic CD.

Building a Theoretical Model Describing Capillary Phenomena in Microchannels in a Plastic CD.

1 Introduction

1.1 Gyros and production of CDs

Gyros AB was formed in 2000 as a spin-off company from Amersham Pharmacia Biotech. The Gyros technology had then been developed during 10 years of research in microfabrication and microfluidics. The aim of the technology platform is to miniaturise common laboratory applications and to develop new applications in microscale by own research. Plastic discs in CD-format in which microstructures have been made are the base for the platform.[1, 2]

The discs are produced by injection moulding of thermoplastic polymers. A master, where the microstructures are formed by an etching process, are used to produce a mould insert (stamper) from which the discs are replicated. Bonding of lid laminates onto the discs seals the microstructures and a capillary network is formed. Solutions are applied through holes in the lids and by utilizing hydrophilic and hydrophobic surfaces, capillarity and centrifugal force, the solutions moves in the microstructures in a controlled and predicted way.[1, 2]

1.2 Contact angles and capillarity

One way to characterise a surface is by the means of the contact angle (θ) of an arbitrary liquid to the surface (see figure 1). The inclination of the tangent of the liquid-gas interface to the plane (or tangent) of the surface at the intersection point (contact line) of gas, liquid and surface gives the contact angle[3].

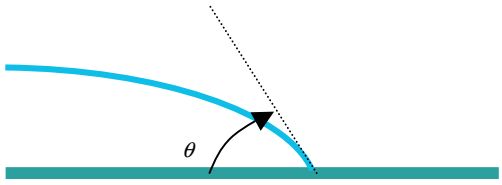

Figure 1 Contact angle (θ) of an arbitrary liquid to a flat surface.

[1] www.gyrosmicro.com/1_0.html (011023)

[2] Andersson P, Dérand H and Hedström A, personal introduction.

[3] Marmur A, Modern Approach to Wettability Theory and Applications, Plenum Press, New York, 327 (1992).

Young's equation (1) gives the cosine of the contact angle as a function of free surface energies, where γ_{SV} refers to the free surface energy of the solid-gas (vapour) interface in the vicinity of the intersection point, γ_{SL} is that of the solid-liquid interface and γ is that of the liquid-gas interface.[4]

$$\cos\theta = \frac{\gamma_{SV} - \gamma_{SL}}{\gamma} . \quad (1)$$

In the theoretical model building section below, the contact angle will be related to a pressure difference over a capillary meniscus. Due to surface properties (roughness and chemical heterogeneity for example) there could be considerable difference between the macroscopic, apparent, and the microscopic, intrinsic, contact angles. That is however of lesser relevance here, because the mentioned pressure difference is a consequence of the curvature of the meniscus, which is actually given by the apparent contact angle.[3]

The contact angle of a stationary liquid is called the equilibrium[4] or the static[5] contact angle. Moving liquids possess contact angles others than the static contact angle. The contact angle can change with time or can be influenced by the flow rate of the liquid and is therefore occasionally called the dynamic contact angle. The contact angle of an advancing liquid on a given surface is called the advancing angle of the surface and that of a withdrawing liquid is called receding angle. The difference of the advancing angle and the receding angle can be 20° or even more. This phenomenon is called contact angle hysteresis and can be explained by e.g. roughness or chemical heterogeneity of the surface.[3, 4, 6]

If the contact angle of water to a surface is more than 90° the surface is considered to be hydrophobic, whereas a surface with a contact angle less than 90° it is considered to be hydrophilic. A capillary of a hydrophilic surface will show capillarity, but a hydrophobic will not.[2, 3] Capillarity is a consequence of different pressures in different parts of the liquid filling a capillary system. The liquid moves in the system in order to reduce these pressure differences. Once the pressures are balanced there will be no more spontaneous flow of liquid.[7] The flow rate of a liquid in a capillary depends on the contact angles, but trying to predict flow rates through the contact angles can be difficult if the surface in question is rough or chemically heterogeneous[3, 4].

The microscopic liquid front in capillaries can assume different shapes depending on the flow conditions. At low contact angles there is a precursor film preceding the macroscopic

[4] de Gennes P G, Reviews of Modern Physics, 828 (1985).
[5] Handique K, Burke D T, Mastrangelo C H and Burns M A, Analytical Chemistry, 4107 (2000).
[6] Brandon S and Marmur A, Journal of Colloid and Interface Science, 351 (1996).
[7] Kim E and Whitesides G M, Journal of Physical Chemistry B, 855 (1997).

liquid front.[4] This precursor film is a few hundred Ångströms thin and has a wedge-like appearance with the absolute front extended to an even thinner film (less than a hundred Ångströms). The extension of the front film is higher at lower contact angles and vice versa.[7]

In the thin front film there can be considerable energy losses due to viscous dissipation and viscosity influencing the flow rate of the liquid[4]. The latter can possibly be observed even though the viscosity can be neglected in the macroscopic flow[8].

In the macroscopic part of the liquid front it has been observed that the liquid imbibies the surface with a rolling wetting mechanism. This mechanism can be compared to the rolling motion of caterpillar treads. With such a wetting mechanism there can also be energy dissipation in the macroscopic front due to the viscosity of the moving liquid.[4] It has been suggested that this rolling wetting mechanism can result in pockets of air close to the surface when flow rates are high (i.e. low contact angles)[8].

1.3 The scope of this work

The aim of this work is to produce a theoretical model for the capillary flow in the microchannel network on the discs. This model would be a valuable tool when designing new structures and channels for future applications. Contributions to the general understanding of the microfluidics in the discs is another aim of this work.

To evaluate the relevance of the theoretic model a range of experiments will be performed and the results will be compared to calculations based on the model. This comparison will include the examination of the impact of surface properties (i. e. the contact angle) and channel dimension on liquid flow rate.

This will initially be achieved by demonstrating capillarity in the discs, secondly by studying spontaneous capillary flow and finally by studying capillarity under external influences (i.e. forced capillary flow).

[8] Kylberg G, personal communication.

2 Building a theoretical model

Since horizontal capillaries are studied, contributions from gravitation will be neglected throughout this work.

2.1 Spontaneous capillary flow in channels with different cross sections

A capillary exerts a force (F) on the meniscus of a liquid inside the capillary. The force depends on the surface tension of the liquid (γ), the contact angle of the liquid to the capillary surface (θ) and x, the perimeter of the capillary (i.e. the contact distance of the meniscus to the capillary) as[3]:

$$F = \gamma x \cos\theta \,. \tag{2}$$

In a capillary, with multiple (n) walls with width x_i , the total force (F_t) on the meniscus can be expressed as a sum of the forces exerted from each of the walls[9]:

$$F_t = \sum_{i=1}^{n} \gamma x_i \cos\theta_i \,. \tag{3}$$

In the following an arbitrary rectangular channel in a CD provided with an arbitrary lid is considered. The properties of the formed capillary taken into account are the width and the depth of the channel (b and d respectively) and the contact angles of the capillary surfaces, which are the contact angles of the disc and the lid (θ_d and θ_l respectively). Given the cross-section area (A) of the channel, the pressure difference over the meniscus (ΔP_m) can be written[10]:

$$\Delta P_m = \frac{F_t}{A} = \frac{\sum_{i=1}^{n} \gamma x_i \cos\theta_i}{bd} = \gamma \frac{(2d+b)\cos\theta_d + b\cos\theta_l}{bd} \,. \tag{4}$$

The liquid pressure (P_m) near the meniscus is given by the atmospheric pressure (P_A) and the pressure difference over the meniscus according to

$$P_m = P_A - \Delta P_m \,. \tag{5}$$

[9] Holmqvist C, Små vätskevolymer i ett centrifugalfält, ÅF-I-Rapport B518, 15 (1999).

[10] Nordling C and Österman J, Physics Handbook, Studentlitteratur, Lund, 153 (1996).

The negative sign in expression 5 is due to the curvature of the meniscus. Since the capillary surface is hydrophilic there is a pressure drop over the meniscus[8].

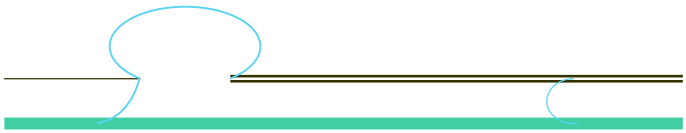

Figure 2 Sketch of liquid entering a channel from an applied drop.

In a situation as the one described in figure 2, the increase in pressure (ΔP_d) over the air-liquid interface in an applied drop at the inlet, where γ is the surface tension of the liquid and R is the radius of the drop, is expressed as[10]:

$$\Delta P_d = \frac{2\gamma}{R}. \tag{6}$$

In accordance with expression 5 the liquid pressure (P_d) near the applied drop is written:

$$P_d = P_A + \Delta P_d. \tag{7}$$

Capillary penetration is a consequence of pressure difference in different parts of the moving liquid. This pressure difference (ΔP) can be expressed as:

$$\Delta P = P_d - P_m. \tag{8}$$

Now, combining expressions 4 – 8 gives:

$$\Delta P = P_A + \Delta P_d - \left(P_A - \Delta P_m\right) = \Delta P_m + \Delta P_d = \gamma \frac{(2d+b)\cos\theta_d + b\cos\theta_l}{bd} + \frac{2\gamma}{R}. \tag{9}$$

Assuming a laminar flow of a Newtonian liquid and that the non-liquid-filled part of the capillary is filled with a fluid of negligible viscosity, the pressure difference (ΔP) across the liquid with viscosity (η) and an average flow rate (v) at a distance (l) from the inlet, can also be expressed as[3, 7]:

$$\Delta P = \frac{32\eta l v}{D^2}. \tag{10}$$

The hydraulic diameter (D) is a parameter given by the area (A) and the perimeter (O) of the cross-section of the capillary according to[8]:

$$D = \frac{4A}{O} = \frac{4bd}{2(b+d)} = \frac{2bd}{b+d}. \tag{11}$$

The shape of an applied drop can be approximated to a half sphere. The radius of a half sphere with a given volume (V) is:

$$R = \sqrt[3]{\frac{3V}{2\pi}}. \tag{12}$$

The contribution from ΔP_d to ΔP depends on the radius of the applied drop according to equation 6. The volume that defines the radius of an applied drop according to equation 12 is determined by the applied volume (V_a) and the volume transported into the capillary (V_d). Thus equation 12 can be rewritten to:

$$R = \sqrt[3]{\frac{3(V_a - V_d)}{2\pi}}. \tag{13}$$

The volume of the liquid transported into the channel (V_d) is simply given by:

$$V_d = bdl. \tag{14}$$

Now, combining expressions 9, 10, 13 and 14 gives

$$\Delta P = \frac{8\eta l v (b+d)^2}{b^2 d^2} = \gamma \frac{(2d+b)\cos\theta_{da} + b\cos\theta_{la}}{bd} + 2\gamma \sqrt[3]{\frac{2\pi}{3(V_a - bdl)}}. \tag{15}$$

Since the liquid now is considered to be in motion, the static contact angles of the disc and the lid are replaced by their corresponding advancing angles, θ_{da} and θ_{la} respectively. To express the average flow rate expression 15 can be rearranged into:

$$v = \frac{b^2 d^2 \gamma}{4\eta l (b+d)^2}\left[\frac{(2d+b)\cos\theta_{da} + b\cos\theta_{la}}{2bd} + \sqrt[3]{\frac{2\pi}{3(V_a - bdl)}}\right]. \tag{16}$$

Due to the production process of the CDs the cross section of the channels is not strictly rectangular. The top of the sidewall tends to be rounded off resulting in extra contact distance (r) to the lid on each side (figure 3).

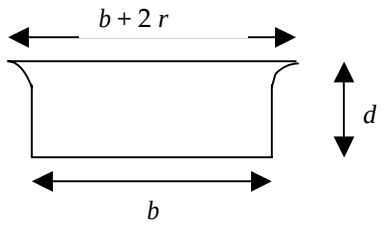

Figure 3 Micro channel shape on CD

As a result the length of the sidewall has to be written:

$$d' = d - r + \frac{\pi r}{2} = d + r\left(\frac{\pi}{2} - 1\right). \tag{17}$$

This influences the perimeter and the cross-section area according to:

$$O' = 2b + 2r + 2d + r(\pi - 2) = 2\left(b + d + \frac{\pi r}{2}\right), \tag{18}$$

$$A' = bd + \frac{r^2}{2}(4 - \pi). \tag{19}$$

Taken this into account expression 16 has to be rewritten to:

$$v = \frac{\gamma A'^2}{\eta l O'^2}\left[\frac{(2d' + b)\cos\theta_{da} + (b + 2r)\cos\theta_{la}}{2A'} + \sqrt[3]{\frac{2\pi}{3(V_a - A'l)}}\right] =$$

$$= \frac{\gamma\left(bd + \frac{r^2}{2}(4 - \pi)\right)^2}{4\eta l\left(b + d + \frac{\pi r}{2}\right)^2}\left[\frac{(2d + r(\pi - 2) + b)\cos\theta_{da} + (b + 2r)\cos\theta_{la}}{2bd + r^2(4 - \pi)} + \sqrt[3]{\frac{2\pi}{3\left(V_a - l\left(bd + \frac{r^2}{2}(4 - \pi)\right)\right)}}\right] \tag{20}$$

2.2 Capillary flow in channels with changing cross section under influence of an applied negative pressure

In this section, a straight channel with a dimension change is to be considered; a narrower channel widens while the depth remains unchanged (from section B to C in figure 4). The depth of the channel is called *d* and the width of section B and C are called b_1 and b_2 respectively. Calling the cross section of section B for A_1 and that of section C for A_2, the following can be stated for the cross sections, the flow rate and the total volume of liquid (*V*):

$$A_1 = b_1 d\ , \tag{21}$$

$$A_2 = b_2 d\ , \tag{22}$$

$$A_1 \frac{dx}{dt} = A_2 \frac{dy}{dt}\ , \tag{23}$$

$$A_1 x + A_2(-y) = V\ , \tag{24}$$

where *x* and *y* are distances from the transition from B to C to the left and right meniscus respectively (see figure 4). Positive x-direction is taken to be to the left in figure 4.

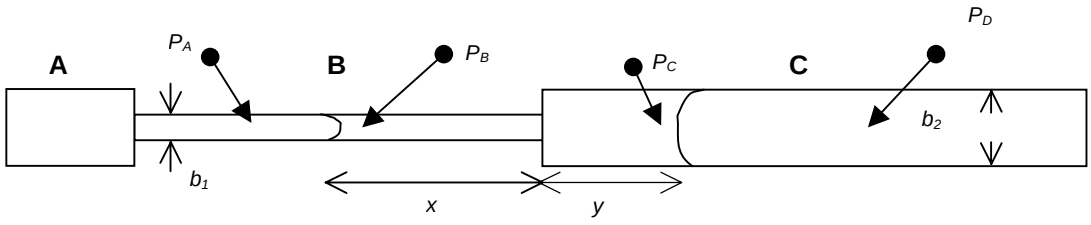

Figure 4 Definition of distances and pressures used in the theoretical model.

The pressure P_A is considered to be the atmospheric, whereas P_B and P_C arise from capillary forces on the menisci in accordance with equations 4 and 5. Since P_B and P_C differ there is a pressure difference (ΔP) across the liquid. For a flowing liquid this pressure difference can be expressed with equation 10. In the situation described in figure 4 the liquid will move to the left if P_D is atmospheric, since the smaller meniscus is stronger than the larger. A way to move the liquid in the other direction is to lower the pressure P_D and thereby counteract the propulsion of the smaller meniscus. P_B and P_C are given by:

$$P_B = P_A - \Delta P_B, \tag{25}$$

$$P_c = P_D - \Delta P_C, \tag{26}$$

where:

$$\Delta P_B = \gamma\left(\frac{(2d + b_1)\cos\theta_d + b_1\cos\theta_l}{db_1}\right), \tag{27}$$

$$\Delta P_C = \gamma\left(\frac{(2d + b_2)\cos\theta_d + b_2\cos\theta_l}{db_2}\right). \tag{28}$$

θ_d and θ_l refers to the contact angles of the disc and lid respectively. P_D is given by equation 29 where P_{ap} is an applied negative pressure:

$$P_D = P_A - P_{ap}. \tag{29}$$

A simple and perhaps the most obvious way to study the capillary forces in this system is to examine at which pressure P_D the upper and lower meniscus are balanced. In that case there should be no pressure drop over the liquid and the equations 30 - 32 holds true according to expressions 25, 26 and 29:

$$P_B = P_C, \tag{30}$$

$$P_A - \Delta P_B = P_A - P_{ap} - \Delta P_C, \tag{31}$$

$$P_{ap} = \Delta P_B - \Delta P_C. \tag{32}$$

Combining equations 27, 28 and 32 gives:

$$P_{ap} = \gamma\left(\frac{(2d + b_1)\cos\theta_d + b_1\cos\theta_l}{db_1} - \frac{(2d + b_2)\cos\theta_d + b_2\cos\theta_l}{db_2}\right). \tag{33}$$

Due to the contact angle hysteresis, an upper and a lower limit for the required applied pressure to balance the menisci can be determined. The upper limit is the negative pressure (P_{apu}) that can be applied without making the liquid move to the right in figure 4. That is, if a higher negative pressure is applied, the liquid will start moving to the right. At this limit the advancing angles of the larger meniscus and the receding angles of the smaller meniscus are considered. The lower limit is the lowest negative pressure (P_{apl}) required for not letting the

liquid move to the left in figure 4. Now, the advancing angles of the smaller meniscus and the receding angles of the larger meniscus are considered. Hence:

$$P_{apu} = \gamma\left(\frac{(2d+b_1)\cos\theta_{dr} + b_1\cos\theta_{lr}}{db_1} - \frac{(2d+b_2)\cos\theta_{da} + b_2\cos\theta_{la}}{db_2}\right), \tag{34}$$

$$P_{apl} = \gamma\left(\frac{(2d+b_1)\cos\theta_{da} + b_1\cos\theta_{la}}{db_1} - \frac{(2d+b_2)\cos\theta_{dr} + b_2\cos\theta_{lr}}{db_2}\right). \tag{35}$$

Another approach to study the capillarity in the system is to observe the flow and relate it to the theoretical model. Here expression 10 is used to formulate a differential equation, which is solved to get the distance dependence of time ($t(x)$) . In other words the time it takes for the smaller meniscus to move a certain distance. (The solution that gives the time dependence of the distance is not as easy to interpret and results in complex roots, which is highly undesirable in this case.)

Using expression 10 the following can be written:

$$\frac{32\eta}{D_1^2}x\frac{dx}{dt} + \frac{32\eta}{D_2^2}(-y)\frac{dy}{dt} = 32\eta\left[\frac{x}{D_1^2}\frac{dx}{dt} + \frac{(V - A_1x)A_1}{D_2^2A_2A_2}\frac{dx}{dt}\right] = \Delta P, \tag{36}$$

where ΔP and the parameters D_1 and D_2 are given by:

$$\Delta P = P_C - P_B = \gamma\left(\frac{(2d+b_1)\cos\theta_{da} + b_1\cos\theta_{la}}{db_1} - \frac{(2d+b_2)\cos\theta_{dr} + b_2\cos\theta_{lr}}{db_2}\right) - P_{ap}, \tag{37}$$

$$D_1 = \frac{4A_1}{2(b_1+d)}, \tag{38}$$

$$D_2 = \frac{4A_2}{2(b_2+d)}. \tag{39}$$

D_1 and D_2 are the hydraulic diameters for the B- and C-section respectively.

Putting

$$\Delta P' = \frac{\Delta P}{32\eta}, \tag{40}$$

and rearranging gives:

$$\left(\frac{1}{D_1^2} - \frac{A_1^2}{D_2^2A_2^2}\right)x\frac{dx}{dt} + \frac{A_1V}{D_2^2A_2^2}\frac{dx}{dt} = \Delta P'. \tag{41}$$

Defining two constants K_1 and K_2 as:

$$K_1 = \frac{1}{D_1^2} - \frac{A_1^2}{D_2^2A_2^2}, \tag{42}$$

$$K_2 = \frac{A_1V}{D_2^2A_2^2}. \tag{43}$$

Rearranging gives:

$$x dx + \frac{K_2}{K_1} dx = \frac{\Delta P'}{K_1} dt \,. \tag{44}$$

Integrating expression 44 and rearranging results in:

$$x^2 + \frac{2K_2}{K_1} x = \frac{2\Delta P'}{K_1} t + C \,, \tag{45}$$

where *C* is an arbitrary integration constant.

Resolving *t* gives:

$$t = \frac{1}{2\Delta P'} \left(K_1 x^2 + 2K_2 x \right) + C' \,, \tag{46}$$

where *C'* is another arbitrary constant.

The condition

$$t(x_0) = 0 \,, \tag{47}$$

gives *C'* according to:

$$C' = \frac{-1}{2\Delta P'} \left(K_1 x_0^2 + 2K_2 x_0 \right). \tag{48}$$

Exchanging *C'* with expression 48 in equation 46 results in:

$$t(x, x_0, P, V) = \frac{1}{2\Delta P'} \left[K_1 \left(x^2 - x_0^2 \right) + 2K_2 \left(x - x_0 \right) \right]. \tag{49}$$

The *x(t)*-solution is obtained in a similar fashion and will be presented but not considered further:

$$x(t, x_0) = \sqrt{\frac{2\Delta P'}{K_1} t + \left(x_0 + \frac{K_2}{K_1} \right)^2} - \frac{K_2}{K_1} \,. \tag{50}$$

2.3 Rotational frequency necessary to create a centrifugal field forcing a liquid to pass a hydrophobic break

The centripetal force (F_c) on an object with mass *m* in a rotational field at a distance *r* from the centre of rotation can be expressed as[10]:

$$F_c = m\omega^2 r \,, \tag{51}$$

where ω is the angular velocity.

Consider a body of liquid with length *l* and density ρ in a radial microchannel on a rotating disc with rotational frequency *f* positioned at an average distance *R* from the centre of rotation. The liquid occupies a volume *V* and the channel has a cross-section area A. Due to

the rotation there is a force acting on the liquid resulting in a pressure gradient over the liquid (ΔP_c) according to:

$$\Delta P_c = \frac{F_c}{A} = \frac{\rho V \omega^2 R}{A} = \rho l \omega^2 R = \rho l 4\pi^2 f^2 R \,. \tag{52}$$

This pressure gradient causes the liquid to move. The motion is also influenced by the forces from the capillary walls acting on the 'front' and 'rear' meniscus. These forces are causing a pressure difference across the menisci expressed as in equations 53 and 54, where ΔP_f and ΔP_r are the pressure drops over the front and rear meniscus, γ the liquid surface tension, θ_{da} and θ_{la} are the advancing angles of the disc and the lid, θ_{dr} and θ_{lr} are the receding angles of the disc and the lid and *b* and *d* are the width and the depth of the channel[11]:

$$\Delta P_f = \gamma \frac{(2d+b)\cos\theta_{da} + b\cos\theta_{la}}{bd}, \tag{53}$$

$$\Delta P_r = \gamma \frac{(2d+b)\cos\theta_{dr} + b\cos\theta_{lr}}{bd}. \tag{54}$$

Since the pressure drop over the rear meniscus is counteracting the pressure gradient due to rotation and the pressure drop over the front meniscus, the following condition for liquid motion can be written:

$$\Delta P_c + \Delta P_f > \Delta P_r \,. \tag{55}$$

To set the liquid in motion by rotating the disc equation 56 must be valid for the rotational frequency, where f_c is the lowest frequency necessary to set the liquid into motion, called the critical rotational frequency:

$$f > f_c \,. \tag{56}$$

The critical rotational frequency can be expressed in other parameters using the inequality (55):

$$\Delta P_c = \Delta P_r - \Delta P_f \,. \tag{57}$$

Expression 52 - 54 and 57 gives:

$$\rho l 4\pi^2 {f_c}^2 R = \gamma \frac{(2d+b)(\cos\theta_{dr} - \cos\theta_{da}) + b(\cos\theta_{lr} - \cos\theta_{la})}{bd}. \tag{58}$$

Rearranging (58) gives:

$$f_c = \frac{1}{2\pi}\left(\frac{\gamma}{\rho l R b d}(2d+b)(\cos\theta_{dr} - \cos\theta_{da}) + b(\cos\theta_{lr} - \cos\theta_{la})\right)^{1/2}. \tag{59}$$

[11] Holmvist C, Critical Rotational Speed, Working paper AP Biotech, 2 (2001).

3 Experimental section.

Calculations were initially (sections 4.1.2 – 4 and 4.3) done in Excel 2000 (Microsoft) but later (section 4.2) Mathcad Professional 2000 (MathSoft) was used. The earlier calculations in Excel were also later performed in Mathcad. (See Mathcad-files in appendix 1.)

3.1 Materials and methods

Discs were mainly made of PC (Polycarbonate, Bayer), but PMMA (Poly(methylmeth-acrylate), Röhm) was occasionally used.

Static, advancing and receding contact angles were measured with a NRL C.A. Goniometer (Ramé-hart, Inc.).

To vary the contact angle of the disc surfaces, the discs were exposed to different oxygen plasma treatments (PS 0500, Plasma Science). Before the plasma treatment the discs were washed in 95% EtOH. Three kinds of surfaces were evaluated: full plasma treated, medium plasma treated and untreated. The parameters for the plasma treatment were: gas flow of 5 sccm and a field strength of 500 W for 10 minutes (full plasma treatment) or gas flow of 10 sccm with a field strength of 100 W for 4 minutes (medium). The medium plasma treated discs were washed with 70 % EtOH after the plasma treatment. The advancing angles of the different discs were determined.

The capillarity of the discs were examined with a cibacron red solution (25 mg Cibacron Brilliant Red (CIBA limited) to 80 ml Milli-Q water (Millipore)). Capillary penetration was studied using a digital video system with a time resolution of 40 ms (Sony DHR-1000NP and Sony GV-300E Digital Video Cassette Recorder). The average flow rate of the advancing liquid at a certain distance (l) from the edge of the lid was determined by measuring distances on a monitor (initially by hand with a ruler, then to get more accurate readings with the software analySIS (Soft Imaging System GmbH)) and using the timer of the video system.

Since cibacron red does not possess any significant surface activity, the surface tension of pure water was assumed[12]. Neither was the viscosity or the density of the coloured water assumed to be markedly affected by the colorant compared to pure water. The viscosity (η), surface tension (γ) and the density (ρ) of water are 8.91×10^{-4} Ns/m^2, 0.0728 N/m and 1000 g/l, respectively [13].

[12] Fielden M, personal communication.

[13] Atkins P W, Physical Chemistry 6:th edition, Oxford University Press, Oxford (1998).

3.2 Spontaneous capillary flow

3.2.1 Demonstrating capillarity

To examine if capillarity could be observed in channels with plastic surfaces, rectangular microchannels with all four sides made of PC or PMMA were constructed. For these experiments CDG1-discs were used. This disc contains rectangular, straight channels with a depth of 60 µm and widths of 60 µm (channels 5 – 8), 120 µm (channel 1 – 4 and 9 – 12), 150 µm (long channel 20) and 250 µm (channels 13 – 19 and short channel 20). The disc design is seen in figure 5.

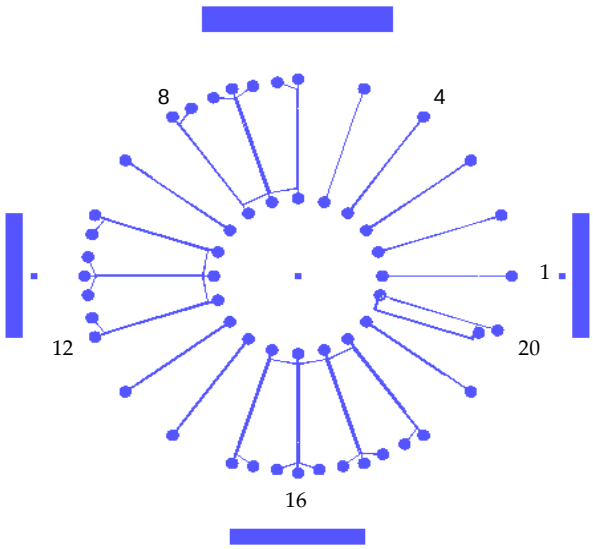

Figure 5 Design of CDG1.

The discs were washed with 90% EtOH and placed on a flat glass plate that had been pre-treated with Repel-Silane ES (Pharmacia Biotech). On the discs, lids cut from blank PC- or PMMA-discs and washed with 95% EtOH, were positioned according to figure 6 A. On top of the lids another silanated glass plate was placed. The lids were bonded onto the discs by applying a weight of a few kilograms on the top glass plate (figure 6 B) and heating the construction in an oven for ~15 h. Bonding temperature was 150 °C and 110 °C for PC and PMMA, respectively.

Capillarity was examined by applying coloured water to the formed channels and noting imbibition. The water was applied with regular pipette tips or GELoader tips (Eppendorf).

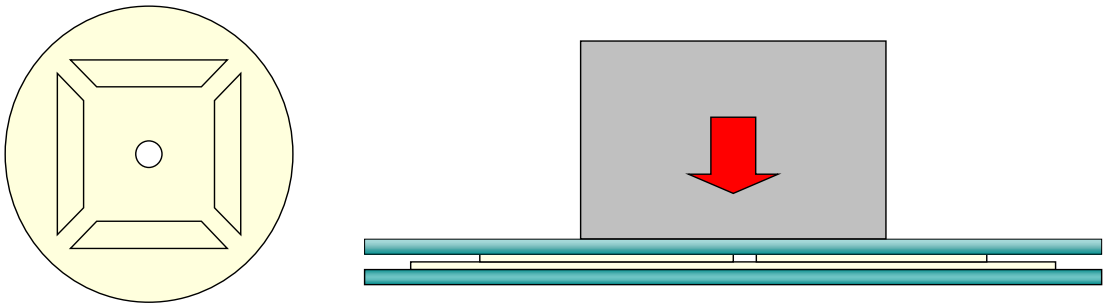

A B

Figure 6 A Sketch of lid placement on the CDG1-disc (not in scale). **B** Sketch of the set-up for bonding lids onto the discs (not in scale). The disc with the lids is positioned between two silanated, flat glass plates and a weight of a few kilograms is applied on the top glass plate.

3.2.2 Channels with different cross sections

To be able to examine the influence of different channel-dimensions on the capillary flow rate, straight channels with design according to table 1 was milled on CDs of PC and PMMA.

Width (µm)	**Depth** (µm)					
200	50	100	150	250	350	500
500	50	100	150	250	500	800

Table 1 Design of milled channels on PC and PMMA discs. All structures were made in triplets.

Lids were bonded onto the discs as in section 3.2.1, but with an additional wash-step with water and detergent before the EtOH-wash

The static contact angles on the two discs were measured before washing, after washing and after the bonding of the lids.

3.2.3 Influence of contact angle and channel dimension on flow rate

Again CDG1-discs were used. Since this disc contains channels with a constant depth and various widths, it is suitable for generating data series, where the influence of the channel dimension can be studied.

Discs with three kinds of surface modifications were prepared: full plasma treated, medium plasma treated and untreated. The static and advancing contact angle of the different discs were determined.

The discs were combined with three different lid laminates characterised by different contact angles (Lid 1, Lid 2 and Lid 3a), with lid design as in figure 6 A. The outer corner angles are 45° and the long sides measure 28 and 44 mm. The lids were fit onto the discs with pressure and heat. The advancing angles of the laminates were previously determined to 77°, 86° and 106° respectively[14].

[14] Wallenborg S, Internal report, Gyros AB.

In a first round of experiments two discs of each surface treatment (full, medium and none; six discs in total) were prepared to cover the whole range of disc, lid and channel combinations. One disc of each surface treatment got Lid 1-lids and the other got Lid 2 and Lid 3a-lids.

At the time for the experiment there were unfortunately no efforts made to keep the distance *l* fixed from test to test. For the calculations *l* was assumed to be 8 mm.

Furthermore, five discs of each surface-treatment-lid-combination (5 x 3 x 3; 45 discs in total) were prepared.

3.2.4 Improved method to study the influence of contact angle and channel dimension on flow rate

Since the test results from sections 3.2.3 showed far to large deviations to be acceptable, an effort had to be made to improve the test quality. Discs with lids covering the whole disc, instead of the smaller lids previously used, were tested. In these tests structures L and M of the CDG12-discs were used. The structures L and M are mainly straight channels with dimensions (depth x width) specified to 100 μm x 400 μm and 40 μm x 200 μm respectively (see figure 7).

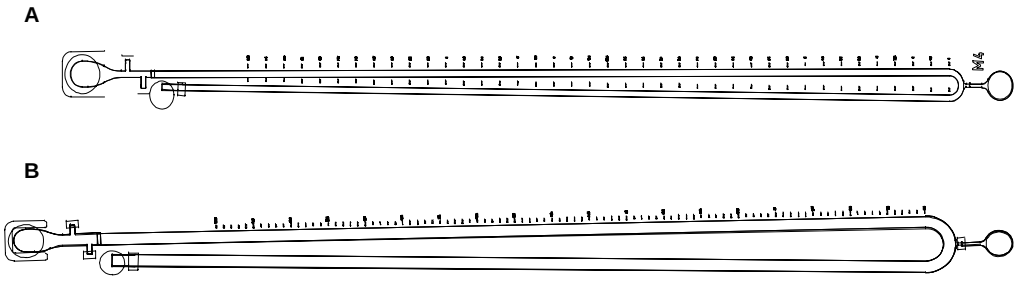

Figure 7 Sketches of structures M (A) and L (B)

Again three kinds of surface modifications were studied: full plasma treated, medium plasma treated and untreated discs. The discs were prepared as described in section 3.1 with one exception: the medium plasma treated discs were treated for 5 minutes instead of 4. The advancing angles (θ_d) on the disc surfaces were measured. The discs where combined with the same types of lid laminates as in 3.2.3 (Lid 1, Lid 2 and Lid 3b). The lids were fit onto the discs with high pressure and heat (Lid 1: 135 °C, Lid 3b and Lid 2: 120 °C) for 0.5 seconds[15]. Capillary penetration into the structures L and M where studied. The applied volume (V_a) of coloured water was 1.5 μl for the L-structure and 1 μl for the M-structure.

[15] In accordance with information note on the press (Åmic AB).

Some depths on the CDs are not reproduced as specified, since the production process is optimised to a channel with dimensions of 100 μm x 500 μm. Changing those parameters results in deviations from the specified dimensions. For a channel with a width less than 500 μm the actual depth is somewhat less than specified. The opposite holds true for channels wider than 500 μm. The extent of deviation is not fully examined, but a depth (*d*) of 35 μm for the M-structure and an unchanged depth for the L-structure are assumed. Considering the 'unsharpening' of the top corners of the channel discussed in the section 2.1, the parameter *r* is known to be approximately 10 μm[16]. The length-parameter *l* is determined by the position of measuring, which was 17 mm for the L-structure and 14 mm for the M-structure.

To get a better picture of the surface properties of the tested and untested structures, SEM-images of the discs and the lids were made (LEO 440 equipped with LaB6 filament, LEO Electron Microscopy Ltd.).

3.3 Capillary flow in channels with changing cross section under influence of an applied negative pressure

In order to examine capillary interaction between a smaller and a larger meniscus, the behaviour of a small volume of liquid in structures D 7 – 9 on the CDG3-disc were studied.

CDG3-discs made of PC were exposed to full plasma treatment. After the plasma treatment the discs were washed with 70% EtOH and the waste channel belonging to structures D 4 – 12 (approximately) was marked with an OH-pen to give the surface in the channel a more hydrophobic quality. Pieces (3 x 5 cm) of Lid 3c-laminate were applied to the discs with pressure and heat (~120 °C). The laminate pieces were applied so that a hole with a diameter of 850 μm (drilled) were positioned on top of the waste channel in the vicinity of structure D 4. To provide the structures to be tested with an inlet, a scalpel was used to remove the lid from a small area on top of structures D 7 – 9 (see figure 8).

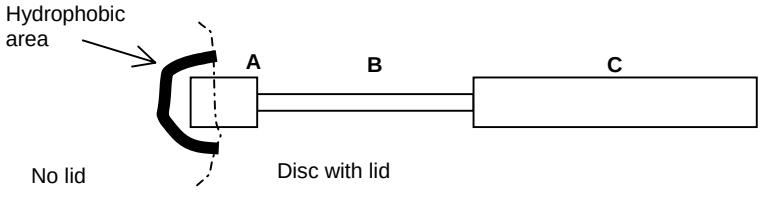

Figure 8 Sketch of structure D 7 – 9 of CDG3 (not in scale). The dashed line shows where the cut with scalpel was done when removing the lid.

[16] Andersson P, personal communication.

The dimensions of structures D 7 – 9 are shown in table 2.

	A	B	C
Width (µm)	250	83.3	250
Length (µm)	500	1500	2000
Depth (µm)	90	90	90

Table 2 Dimensions of structures D 7 – 9. Designations A – C refers sections defined in figure 8.

By applying vacuum through the hole over the waste channel a hydrophilic coating-solution were applied and forced into the structures. The coating-solution was removed after approximately five minutes. This surface treatment alters the advancing angle of the lid from 106° to 104° and the reversing angle of the lid changes to 77° [14]. The advancing and the receding angles of a hydrophilic coated disc were measured.

Coloured (cibacron red) water was applied to the inlet with a needle carrying an approximate volume of 50 nl. Trying to prevent the liquid from escaping the structures by wicking and subsequent evaporation, a hydrophobic mark was applied around the inlet with an OH-pen according to figure 8. The liquid was forced into the structure with an applied negative pressure by connecting a vacuum pump (1500 DV, EFD) to the hole over the waste channel. The resulting pressure was measured with a vacuum indicator (VD 81 EX, Thyracont). The applied volumes were determined by measuring the length of the channel that the liquid occupies and multiply it with the cross section area.

3.4 Rotational frequency necessary to create a centrifugal field forcing a liquid to pass a hydrophobic break

In a number of experiments (the so called 'standardtest') the functionality of hydrophobic breaks in microchannels has previously been examined. A coloured liquid is loaded onto a disc and capillarity causes the liquid to penetrate into microchannels on the disc. The cross section of the channel is rectangular-shaped with three sides from the disc and the fourth from the lid. The surface properties are described by the contact angles θ of the disc (*s*) and the lid (*l*), i. e. the advancing angles θ_{da} and θ_{la} and the receding angles θ_{dr} and θ_{lr} (table 3).

	Lid 3d	Lid 3d + hydrophilic coating	Lid 1	Lid 1 + hydrophilic coating	Disc	Disc + hydrophilic coating	Break
Advancing angle (°)	104	90	77	43	4	36	116
Receding angle (°)	78	46	48	15	2	24	88

Table 3 Advancing and receding angles for the materials involved.[17]

The liquid penetrates the channel until the liquid front reaches a hydrophobic break where it stops. Now, when spinning the disc the liquid can pass the break at a certain critical rotational frequency (f_c), which is registered.

For these tests the structure A on CDG10-discs has been used. The A structure is a mainly straight channel with a width of 200 μm and a specified depth of 40 μm. In accordance with reasoning in section 3.2.4 the depth is assumed to be 35 μm when used in the theoretical model. The position of the hydrophobic break determines the distance from the centre of rotation (R) to 26.5 mm and the length of the formed liquid body (l) to 2 mm.

The data assembled come from previously done experiments[18]. Several types of liquid were used in these tests. The results from tests where coloured water was used, were chosen and studied.

4 Results and discussion

4.1 Spontaneous capillary flow

4.1.1 Demonstrating capillarity

Initially some time was spent trying to optimise the bonding process. A few drawbacks to mention were cracked discs, an apparently oil-impregnated weight causing nasty-smelling, black smoke in the hot oven and an oven with a safety temperature-fuse set to ~100 °C, when 150 °C was required. The cracked discs were not a major problem since most of the structures remained intact and could be tested. The purpose with these tests was to examine if capillarity could be observed in channels without modifications of the plastic surface, because earlier observation suggested it could not[16].

Two types of pipette tips were used when applying the liquid, regular and GELoader tips (Eppendorf). On all PMMA-discs capillarity was observed. For the PC-discs the test results depended on the type of pipette tips used. Application with regular tips occasionally resulted in liquid entering the channel, while application with GELoader tips mostly resulted in

[17] Sources were internal Gyros-reports (break (Dérand H) and lids (Wallenborg S)) and measurements in section 3.1.4 (disc) and 3.3 (hydrophilic coated discs).

[18] Hedström A, Internal report, Gyros AB.

imbibition of the channel. This difference is most probably explained by the way the loading is done using either of the tips. It was observed that on the PC-discs, the liquid had to have contact with all for walls (or rather the four corners) of the channels at the inlet to be able to penetrate into the channel. This is achieved when using GELoader tips, since it is possible to apply the liquid at the bottom of the channel right in front of the inlet. When using regular tips a droplet is placed on the edge of the lid over the channel. In this position the drop has contact with the top wall of the channel (the lid) and parts of the sidewalls, but has no contact with the bottom wall. The rather high contact angle of PC makes it more energetically favourable for the drop to maintain its 'drop shape' than to advance along the walls of the capillary to get contact with the bottom corners and thereby allow capillary imbibition.

4.1.2 Channels with different cross sections

Due to the laborious process only one disc of PC and one of PMMA was prepared to study spontaneous capillarity. In the structures with a depth of 200 μm on the PC-disc there were burrs from the milling. When examining and comparing different structures to each other, smooth surfaces are preferred because roughness influences the capillary flow in a rather unpredictable way. The burrs were removed with scalpel with various results; most of the more shallow structures (depth ≤ 150 μm) got ugly marks from the scalpel. Whether the scalpel marks and the burrs had any impact on the capillary flow is hard to say, since the milling itself results in rough structures (figure 9 - 12). In figure 10 the mentioned scalpel marks can be seen. Since the channel surfaces in these discs were considered too rough, no attempt to determine the flow rate were made.

Figure 9 Milled channel with width 500 μm in PC.

Figure 10 Milled channel with width 200 μm in PC.

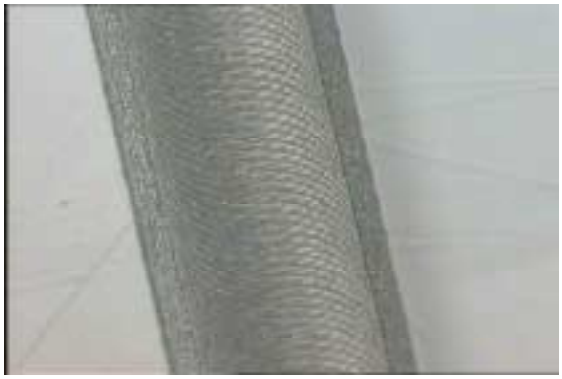

Figure 11 Milled channel with width 500 µm in PMMA.

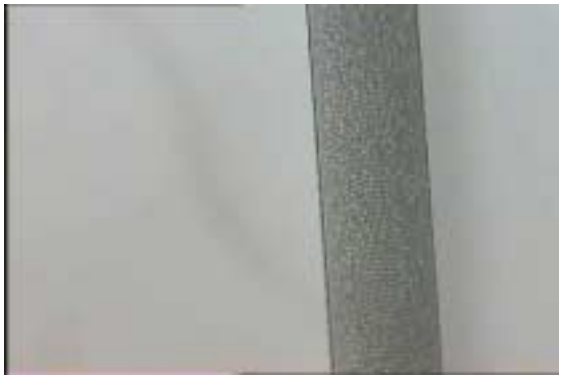

Figure 12 Milled channel with width 200 µm in PMMA.

Table 4 shows the measured static contact angles of the PC and PMMA disc. All measurements are made on the discs between the structures, since it is practically difficult to measure the contact angles in the microchannels.

Measured static contact angle (°, n = 4)			
	Untreated	**Washed with 95% EtOH**	**After heat treatment**
PC	78 ± 4	80 ± 1	81 ± 5
PMMA	68 ± 4	64 ± 2	69 ± 2

Table 4 Measured static contact angles for the PC and PMMA discs. Each measurement was performed 4 (n) times.

The PC-disc cracked after bonding of the lids, but luckily the structures to be tested remained intact. In all structures on the PMMA-disc capillarity was observed. The result from the PC-disc is shown in table 5.

PC			
Depth (µm)	**Width** (µm)	**Pipette tip**	**Capillarity**
500	50	regular (r) GELoader (Gl)	- -
	100	r Gl	- yes, but no complete fill
	150	r Gl	- yes, to 33% of channel length
	250	r Gl	yes, to 20% of channel length yes
	500	r Gl	yes yes, almost completely
	800	r Gl	- yes, almost completely
200	50 - 500	no capillarity observed in any structure	

Table 5 Results from the tested PC-disc with milled structures. Blanks mean no capillarity observed.

It is hard to determine why no capillarity was observed in any of the structures with a depth of 200 μm and some of the other structures. A probable cause is the rough surface, which is a direct result of the milling. Thereto the scalpel marks explained above must be considered.

4.1.3 Influence of contact angle and channel dimension on flow rate

To cover all possible combinations of lids, discs and channels of different dimensions six CDs (PC 7 – 12) were prepared and tested. The measured advancing angles and static contact angles of these discs are presented in table 6.

	Disc					
	Full		Medium		None	
Advancing angle (°, n = 3)	9 ± 3	8 ± 1	60 ± 3	59 ± 5	90 ± 3	92 ± 2
Static contact angle (°)	7 - 13	10	59 - 70	37 - 79	79 - 83	72 - 80

Table 6 Measured advancing angles and static contact angles of six discs with different surface treatments. The advancing angles were measured 3 (n) times, whereas the number of measurements for the static contact angles were not registered.

The static contact angles were measured on the discs after the lid had been applied. The probable explanation for the huge variation in these measurements is that the disc surfaces have been affected by the press used when applying the lids.

Some of the structures on the CDG1-disc are designed with one or two adjacent channels, namely the structures 6 – 8, 10 – 12 and 15 – 18 (see figure 5). For these structures the production of the discs or the application of the lid were not optimal, resulting in a free space between the lid and the wall separating the channels. As a consequence the liquid also filled the channels adjacent to the channel that was to be tested and thereby unaccountably changed the geometry considered in theoretical model. In these cases the test results were discarded.

The results from the measurements are presented in table 7.

	Lid:	Lid 1	Lid 2	Lid 3a
Plasma treatment	**Channel width**	**Mean flow rate** (mm/s; (n))		
Full	**60**	99 ± 24; (2)		27 ± 2; (2)
	120	110 ± 10; (3)	98; (1)	39 ± 14; (4)
	150			29; (1)
	250	109 ± 30; (2)	74 ± 21; (3)	29 ± 1; (2)
Medium	**60**	2.2; (1)	0.90 ± 0.2; (3)	
	120	0.84 ± 0.4; (4)	7.7; (1)	0.0036 ± 0.0011; (2)
	150	26; (1)		0.030; (1)
	250	36 ± 20; (2)	5.2 ± 0.2; (2)	0.38; (1)
None	**60**	0.37; (1)	0.21 ± 0.11; (8)	
	120	0.31 ± 0.08; (4)		
	150	0.49; (1)		
	250	0.62 ± 0.06; (2)	3.9, (1)	2.2; (1)

Table 7 Average measured flow rates. Blanks mean no result obtained. n refers to the numbers of channels tested.

Due to the low number of data-points it is unwise to draw conclusions from the results presented in table 7. Nevertheless, an observation to be made is that the choice of lid influences the flow rate markedly. In most cases were highest flow rates observed for Lid 1, followed by Lid 2 and finally Lid 3a, given the channel dimension and the surface treatment of the disc. This is in agreement with the theoretical model (see figure 13 A and B), which predicts the highest flow rates for the lid with the lowest advancing angle.

Likewise it is shown in figure 13 A and B that for the dimension-interval studied the theoretical model also predicts the flow rate to increase with increasing channel width and constant channel depth. This is not seen in table 7, indicating the inconsistency of these results. A problem in this situation is that it is hard to determine if the low quality of the result depends on the theoretical model, the experimental setup or both. Generating more data might give the answer.

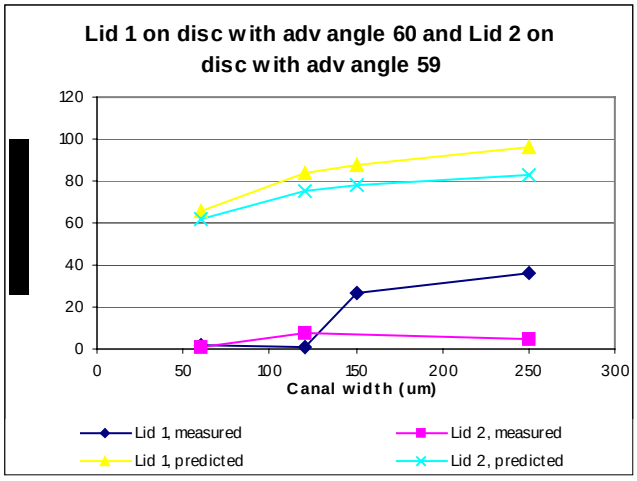

Figure 13 A This graph shows measured flow rates on medium plasma treated discs with Lid 1- or Lid 2-lids (test results presented in table 7) compared to calculated flow rates.

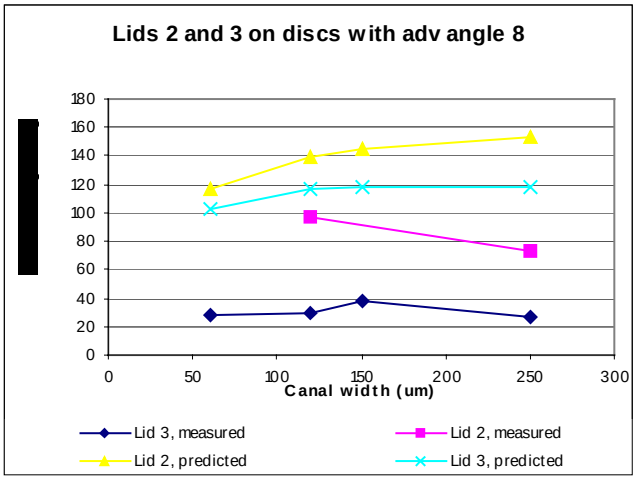

Figure 13 B This graph shows measured flow rates on full plasma treated discs with Lid 2- or Lid 3a-lids (test results presented in table 7) compared to calculated flow rates.

The theoretical model referred to in the paragraph above is a reduced form of expression 16. The formula used to calculate the flow rates demonstrated in figure 13 neglected the last term in expression 16, which derives from the pressure contribution from the drop that was not considered at this time:

$$v = \frac{b^2 d^2 \gamma}{4\eta l (b+d)^2}\left[\frac{(2d+b)\cos\theta_{da} + b\cos\theta_{la}}{2bd}\right]. \qquad (61)$$

It should also be stated that the reasoning about the actual shape of the channel (due to CD-production process, see section 2.1, equation 20) was not considered at this stage.

An additional five discs of each surface-treatment-lid-combination were prepared and tested. Not all possible combinations were tested, since the results generated during the execution of the experiment showed far too large deviations to be considered informative. Therefore the experiment was not completed. The results collected before the abortion of the experiment are presented in table 8 below. It is easily understood that it is impossible to draw any conclusions from these results. The relative deviations are in most cases close to one or above. In order to improve the data quality a new approach was evaluated, where lids covering the whole disc were used.

Plasma treatment:	Medium				None			
Channel width (μm)	**Flow rate** (mm/s)	**Standard deviation**	**Relative deviation**	**n**	**Flow rate** (mm/s)	**Standard deviation**	**Relative deviation**	**n**
Lid 1								
250	2.0	2.5	1.2	12	0.46	0.27	0.59	12
150	0.94	0.51	0.54	3	0.13	0.06	0.46	3
120	0.95	1.2	1.3	14	0.22	0.15	0.68	11
60	3.5	3.5	1.0	10	0.11	0.12	1.1	9
Lid 2								
250	4.0	3.9	0.98	12	0.83	0.50	0.60	12
150	5.8	5.9	1.0	2	0.74	0.58	0.78	3
120	3.0	5.7	1.9	14	0.36	0.25	0.69	13
60	5.0	7.1	1.4	13	0.18	0.12	0.67	13
Lid 3a								
250	0.038	0.051	1.3	10				
150	0.0034			1				
120	0.036	0.052	1.4	7				
60	0.98	1.8	1.8	12				

Table 8 Average measured flow rates. n refers to the numbers of channels tested.

4.1.4 Improved method to study the influence of contact angle and channel dimension on flow rate

Comparing calculations from equation 16 and 20 showed that the changed dimension of the channel due to rounded top corners did not make any considerable difference (data not shown). Therefore expression 16 was used when comparing experimental result to calculated.

The advancing angles (θ_d) for the full plasma treated, the medium plasma treated and the untreated discs were measured to 4°, 44° and 85° respectively. The result from the theoretical calculations and the experiments for structure L and M are presented and compared in table 9 and 10 respectively.

	Disc and lid combinations with advancing angles						
Surface treatment	**None** (85°)		**Medium** (44°)		**Full** (4°)		
Lid	**Lid 1** (77°)	**Lid 2** (86°)	**Lid 1** (77°)	**Lid 2** (86°)	**Lid 1** (77°)	**Lid 2** (86°)	**Lid 3b** (106°)
Calculated flow rate (mm/s)	24.2	18.2	60.6	54.7	76.7	70.7	57.4
Experimental flow rate (mm/s)	0.120 ± 0.069	4.33 ± 1.0	6.30 ± 0.93	9.47 ± 1.6	26.7 ± 1.2	18.5 ± 1.1	21.8 ± 0.96
Quotient between theoretical and experimental flow rate	202	4.20	9.62	5.78	2.87	3.82	2.63

Table 9 Calculated flow rate, experimental flow rate and the quotient between the both for structure L with dimensions 100 x 400 µm.

	Disc and lid combinations with advancing angles						
Surface treatment	**None** (85°)		**Medium** (44°)		**Full** (4°)		
Lid	**Lid 1** (77°)	**Lid 2** (86°)	**Lid 1** (77°)	**Lid 2** (86°)	**Lid 1** (77°)	**Lid 2** (86°)	**Lid 3b** (106°)
Calculated flow rate (mm/s)	8.05	5.18	23.8	21.0	30.8	27.9	21.5
Experimental flow rate (mm/s)	0.400 ± 0.51	0.320 ± 0.24	2.94 ± 0.52	2.65 ± 0.28	11.2 ± 0.43	7.42 ± 0.83	8.66 ± 0.66
Quotient between theoretical and experimental flow rate	20.1	16.2	8.09	7.92	2.75	3.76	2.48

Table 10 Calculated flow rate, experimental flow rate and the quotient between the both for structure M with dimensions 40 x 200 µm.

The calculated flow rates are higher than the measured ones with a factor ranging from 2.48 to 202. A puzzling feature is that the flow rate does not seem to unambiguously depend on the advancing angles of the lid, since the liquid moves faster on a maximum plasma treated disc with a Lid 3b-lid than on a similar disc with Lid 2-lid. This is also the case for the L-structure on the untreated discs. The measured flow rates in the latter case are surprisingly inconsistent considering the huge difference between the two values corresponding to the two lids. It is now tempting to draw the conclusion that these measurements are not representative. Doing so one can see that the factor relating measured values to theoretical varies with disc properties independent of the lid according to: maximum treated discs ~3, medium treated ~8 and untreated ~20. It is important not to over-interpret these numbers since they are results of data with significant statistical errors. This is most obvious for the untreated discs. For clarity it should be stated that tests with the same type of surface and lid are made on the same disc.

Whether the neat factor series is 'true', a coincidence or a product of manipulated data, the obvious approach to explain the non-ideal behaviour of the capillary is to consider the surface property of the lids and the discs. Surface roughness and chemical heterogeneity are

properties that influence the contact angle. To represent these properties in the theoretical model an angle disturbance (α_d and α_l) can be added to expression 16. One can also imagine that the wetting process somehow disturbs the geometry causing the capillary pressure. With a rolling wetting mechanism a layer of air can form between the moving liquid front and the capillary walls, which probably slows the liquid flow down. To account for this, dimension exponents ($\mu 1$ and $\mu 2$) are added to expression16:

$$v = \frac{b^2 d^2 \gamma}{4\eta l (b+d)^2}\left[\frac{[m](2d+b)^{\mu 1}\cos(\theta_d + \alpha_1)}{2bd[m]^{\mu 1}} + \frac{[m]b^{\mu 2}\cos(\theta_l + \alpha_2)}{2bd[m]^{\mu 2}} + \sqrt[3]{\frac{2\pi}{3(V_a - bdl)}}\right].$$

(61)[19]

Unfortunately these additional factors do not contribute to a better general agreement between experiment and the theoretical model no matter how you vary them. In fact, the best result so far to 'correct' the theoretical expression is to multiply expression 16 with a factor ($\cos\theta_d$)/3. The problem is that such a factor is fully arbitrary and has no physical relevance.

Examining the SEMs reveals that the discs have relatively smooth surfaces (see figure 14). So have the lids with one exception: Lid 3b, where the layer of glue seems to contain some kind of particles giving the surface a very rough appearance (SEM not shown).

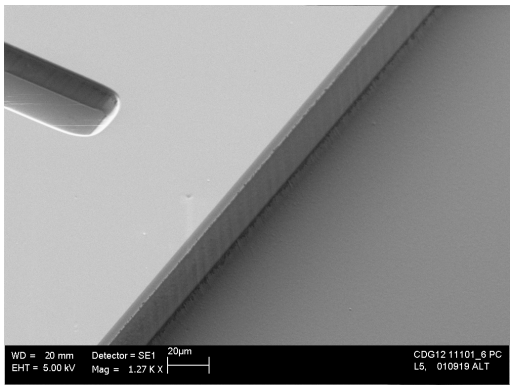

Figure 14 SEM-image showing part of a channel (structure L, not tested) on an untreated PC-disc. The structure is seen in the lower right corner. The upper left half of the image shows the top surface of the disc.

If this was a general characterisation of the Lid 3-lids, then it should have a negative impact on the flow rate. The results from the tests presented in table 9 and 10 do not support this, when they are compared to the results from the tests with the other two lids. However, the SEMs for the Lid 3b-lids are prepared from a medium plasma treated disc and when this disc was tested hardly any capillarity was observed, even though capillarity is expected in that

[19] [*m*] is the length unit meter, included to get the units in the expression right.

case. A further examination of Lid 3-lids should clarify whether the SEMs presented here are representative or not.

4.2 Capillary flow in channels with changing cross section under influence of an applied negative pressure

The advancing and the receding contact angle of the hydrophilic coated discs were measured to 36° and 24°, respectively.

The experiments were performed at an atmospheric pressure of 1009 mbar. When trying to balance both menisci, P_D was measured to approximately 999 (998 – 1000) mbar resulting in an applied negative pressure (P_{ap}) of 10 mbar or 1000 Pa. This lies well within the limits obtained when calculating the pressures P_{apu} and P_{apl}, as seen in table 11.

P_{apu} (Pa)	P_{apl} (Pa)	P_{ap} (Pa)
1590	419	1000

Table 11 Calculation of upper (P_{apu}) and lower (P_{apl}) limits of the applied negative pressure compared to the experimentally applied negative pressure (P_{ap}).

The results from the flow experiments and the corresponding theoretical calculations are showed in table 12 and 13. The flow monitored in the experiments referred to in table 12 is obtained by applying a negative pressure (P_{ap}) outside the larger meniscus and thereby moving the liquid (see figure 4).

Applied negative pressure, P_{ap} (Pa)	Measured x_0 (µm)	Measured x (µm)	Theoretical t (ms)	Experimental t (ms)	Mean flow rate (mm/s)
2100	670	270	1.8	280	1
2100	270	80	0.46	360	0.5
1600	730	50	110	1920	0.4
1200	690	150	-3.1	320	2
1300	760	140	-5.0	280	2
1300	780	140	-5.3	360	2
1200	850	0	-4.9	680	1
1400	700	0	-7.5	160	4
1300	810	70	-5.3	560	1
1300	1060	60	-8.7	400	2
1400	1010	0	-12	200	5

Table 12 Comparing calculated ($t(x_0, x, P_{ap})$) and measured flow times.

In table 13 the flow in the opposite direction is considered. This flow is obtained by shutting off the negative pressure when the smaller meniscus is near the widening of the channel. The

distance from the smaller meniscus to the widening of the channel at time zero is called x_0. The corresponding distance at time t is called x.

Measured x_0 (µm)	**Measured x** (µm)	**Theoretical t** (ms)	**Experimental t** (ms)
70	550	2.0	40
70	940	5.1	40
70	100	6.1	40
280	860	3.9	120
30	810	4.1	40
0	770	3.9	60
0	810	4.2	40
0	680	3.1	40
70	1090	6.2	80
60	1060	5.9	80

Table 13 Comparing calculated ($t(x_0, x)$) and measured flow times.

The results in table 12 may at a first glance seem very confusing. In some aspects they are, but the most obvious peculiarity, the calculated negative times, are explained by examining the pressure contribution ΔP. In equation 48 ΔP is given by the theoretical pressure difference over the liquid due to capillary forces on the menisci and the applied negative pressure. To move the liquid in a way that gives positive values using expression 48 the applied negative pressure must exceed the pressure difference over the liquid. In this case a negative pressure of 1489 Pa or larger is required. As seen in table 12 the liquid is moved at lesser negative pressure, which results in a negative ΔP-contribution to equation 48 and consequently the calculations result in negative values. The dependence of flow time on the applied pressure is showed in figure 15. As seen, the flow time approach infinity when the applied pressure approaches the theoretical pressure difference over the liquid. The interpretation of this is that when the applied pressure equals the pressure difference over the drop, the liquid will not move. It would then take infinite time for the liquid to get from position x_0 to x.

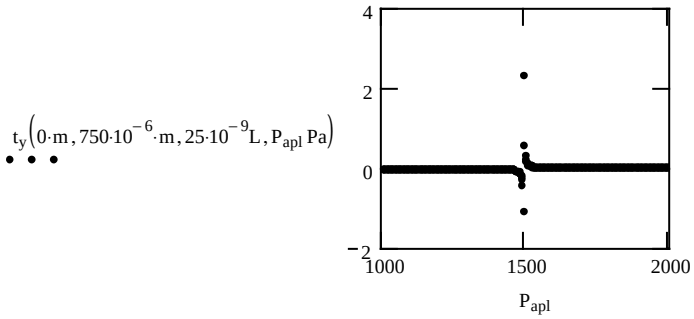

Figure 15 Graph of the dependence of flow time on applied pressure.

Since some of the calculated times are negative, it is difficult to compare these to the experimental and draw any qualitative conclusions. Still it seems that the theoretical model

clearly underestimates the time needed to move the liquid a certain distance. The magnitude of the calculated times are in the order of single milliseconds, while the experimental are in the order of hundreds of milliseconds.

A contribution to these results could be the pressure measurements, which are far from precise. The accuracy achieved with the vacuum meter used was only down to 100 Pa, which is not enough when considering pressure contributions in the size of 1000 Pa as in this case. But since the pressure measurements differ substantially from test to test the inaccuracy in the readings cannot explain the results from the calculations. Ideally, the capillary flow in one type of structure under some fixed applied pressure should behave uniformly, but it does not. It is striking that there is no correlation whatsoever between applied pressure and achieved flow rate (see table 12). This implies that the theoretical model cannot describe capillary flow in a satisfactory way or rather that the experimental setup was far from optimal.

Comparing the calculated and measured times in table 13 reveals that there is a huge difference between the two. The measured times are approximately 14 times the calculated (7 times at the best, 31 at the worst). This is, however, in some agreement with result presented above in sections 4.1.2 - 4, where the theoretical model predicts the liquid to flow a lot faster than it actually does.

An explanation for the extreme results in this case could be that the theoretical model does not account for the fact that the liquid is initially accelerated from a stationary state. Newton's second law can be used to estimate the initial acceleration of the liquid[10]:

$$F = ma\,. \tag{62}$$

Calculations show that the acceleration is around 550 m/s^2, which means that during the time resolution of the experiment (40 ms) the liquid could be accelerated to a flow rate of approximately 22 m/s. This is a flow rate about 1000 times as fast as the observed (see table 12). Consequently the acceleration can be regarded as immediate and will not require to be accounted for in the theoretical model. The lack of acceleration contribution to the theoretical model is at least not an explanation for the inconsistency between theoretical and practical results.

Due to the acceleration of the liquid when passing the widening of the channel there is an additional pressure contribution (P_{acc}) not considered in the theoretical model section according to[8]:

$$P_{acc} = \frac{\rho}{2}\left(\left(\frac{dx}{dt}\right)^2 - \left(\frac{dy}{dt}\right)^2\right). \tag{63}$$

Calculations of this pressure contribution using observed flow rates reveal that it is sufficiently small to be ignored. The other pressures concerned are at least 10 000 times higher than P_{acc}.

Several trials were made to generate the necessary pressure gradient over the liquid by spinning the discs. Unfortunately, it was not possible to achieve any control over the liquid with that approach. The dominating problem in this case was the extensive wicking along the corners of the structures. Thus it was possible to pull (by negative pressure) the liquid in a controlled way, but not to push it (by spinning).

4.3 Rotational frequency necessary to create a centrifugal field forcing a liquid to pass a hydrophobic break

The result from the experiments[18] and the calculation is seen in table 14.

	Critical rotational frequency (rpm)	
	Calculated	**Experimental**
Lid 3d	2950	2840 ± 300 (n=4)
Lid 1	2950	3080
Hydrophilic coating, Lid 3d	3040	2790 ± 320 (n=8)
Hydrophilic coating, Lid 1, hydrophobic breaks on lid	3470	5420

Table 14 Measured and calculated critical rotational frequency for some different lids and surface treatments.

Taken the error margin into account the theoretical values correspond rather well to the measured with one exception; the hydrophobic breaks in discs where also the lid is patterned are far more efficient than the theoretical model predicts.

5 Concluding remarks and suggestions for future work

A first general conclusion is that the theoretical model and reality corresponds rather well in (quasi-) stationary situations. It is possible to predict the rotation frequency necessary to move a liquid over a hydrophobic break with an accuracy that is acceptable. Also calculations of the negative pressure that can be applied to balance a larger and a smaller meniscus corresponds well to the measured pressure. However, as soon as the liquid is set into motion the theoretical model fails and the reasons therefor are not obvious.

When discussed in the literature, the general explanation for lower flow rates than expected is that properties of the surface influence the contact angle. The more rough or chemically heterogeneous the surface, the higher the contact angle and consequently the lower the flow rate. In addition, it cannot be excluded that the actual contact angles in the microchannels differ from the ones measured on the discs. The effect of this deviation of the contact angle was examined. Varying the contact angles in the theoretical model shows that there is no possibility that the deviations in the theoretical model solely can be explained through deviations of the contact angles.

The most attractive guess so far, not including contact angles, is that the wetting process slows down the flow of liquid in a way not predicted by the theoretical model. The liquid front can assume different shapes depending on the flow conditions. During the tests a thin precursor film preceding the advancing meniscus was occasionally observed. It is possible that the wetting process includes energy dissipations in form of heat in the precursor film, which would negatively influences the flow rate. This could be due to viscous dissipations, viscous friction or some other local phenomenon. The precursor film is generally a few hundred Ångströms thin and the viscosity of the moving liquid can give a substantial contribution to the energy dissipation in the precursor film. It is possible that the colourant (cibacron red) can increase the viscosity of the liquid and thereby further increase the energy dissipation. There might also be viscous energy dissipations due to the rolling wetting mechanism.

Another and perhaps somewhat farfetched explanation for the inconsistency between the theoretical model and the experiments is that there could be a solubility process affecting the liquid flow. If it takes considerable time for the water molecules to order themselves to the surface molecules when wetting the surface, it would influence the flow rate.

Today the actual dimensions of the structures studied differs somewhat to the dimensions specified in the design due to the production process. This, of course, is a source

of error when comparing the theoretical model to experiments. Even so, it induces modest errors and cannot alone explain the sometimes huge difference between observed flow rates and calculated.

Of course there is always the possibility that the theoretical model itself contains errors making it unsuitable for this kind of analysis. However, the approach to relate capillary flow rate to a pressure difference in the liquid (equation 10) has been used before with far better agreement with experiments[7].

The theoretical model proposed seems to be able to describe stationary situations in capillaries, but cannot properly describe dynamic ones. In any case this work has contributed to a better understanding of liquid behaviour in the micro channels in the discs. Altogether the aim of this work must be considered to be achieved, although be it not completely.

The natural continuation of this work is to formulate a theoretical model that accounts for the above suggested energy dissipations and to examine whether that theoretical model better predicts liquid flow. Additional experiments should also be performed to achieve better basic data.

Acknowledgements

First of all I would like to express my gratitude to all of the Gyros-staff for making my time at Gyros pleasant. Thank you for your kindness, patience and support. I would especially like to thank Per Andersson for conceptual ideas and encouragement, Helene Dérand, my examiner, for constructive criticism and ideas, Gunnar Kylberg for supporting me with the theoretical model-building, and finally Anders Hedström, my supervisor, who arranged this project, guided me through all the practical parts of it and indeed contributed to the outline of this report.

I also wish to thank Olle Larsson and Anna-Lisa Tiensuu at Åmic AB for providing me with figure 5 (Olle) and figure 14 (Anna-Lisa).

Finally I would like to thank my friends and family for everything. You make me feel good. The most special and warmest gratitude is dedicated to my fiancée Pernilla, who brings about the necessities in my life. You are the best.

Further reading

Anderson R C, Bogdan G J, Puski A and Su X, μTAS, Kluwer Academic, London, 11 (1998).

Bang Cheng S, Skinner C D, Taylor J, Attiya S, Lee W E, Picelli G and Harrison D J, Analytical Chemistry, 1472 (2001).

Dong M and Chatzis I, Journal of Colloid and Interfacial Science, 278 (1995).

Duffy D C, Gillis H L, Lin J, Sheppard, Jr. N F and Kellogg G J, Analytical Chemistry, 4669 (1999).

Hadd A G, Raymond D E, Halliwell J W, Jacobson S C and Ramsey J M, Analytical Chemistry, 3407 (1997).

Hedström A and Togan-Tekin E, Hydrophobic valves in straight channels, Experimental Report Gyros AB (2001).

Holmqvist C, The resistance provided by a dimensional change in a capillary, Working paper AP Biotech (2001).

Jiang Y, Wang P-C, Locascio L E and Lee C S, Analytical Chemistry, 2048 (2001).

Tiberg F, Zhmud B, Hallstensson K and von Bahr M, Physical Chemistry Chemical Physics, 5189 (2000).

Voinov O V, Journal of Colloid and Interfacial Science, 5 (2000).

Zhmud B V, Tiberg F and Hallstensson K, Journal of Colloid and Interfacial Science, 263 (2000).

Appendix 1

Mathcad file for calculation of flow rates (section 4.1):

$b := 400 \cdot 10^{-6} m \quad d := 100 \cdot 10^{-6} m \quad \alpha_{sa} := 85 \quad \alpha_{la} := 86 \quad V_a := 1.5 \cdot 10^{-6} L \quad l := 17 mm$

$\gamma := 0.0728 \frac{N}{m} \quad \eta := 8.91 \cdot 10^{-4} \frac{N \cdot s}{m^2} \quad D := \frac{2 \cdot b \cdot d}{b + d} \quad A := b \cdot d$

$$P_m := \gamma \cdot \frac{(2 \cdot d + b) \cdot \cos\left(\alpha_{sa} \cdot deg\right) + b \cdot \cos\left(\alpha_{la} \cdot deg\right)}{A} \qquad P_m = 145.957 Pa$$

$$P_d := 2 \cdot \gamma \cdot \sqrt[3]{\frac{2\pi}{3 \cdot \left(V_a - b \cdot d \cdot l\right)}} \qquad P_d = 199.026 Pa$$

$$P := P_m + P_d \qquad P = 344.983 Pa$$

$$v := \frac{P \cdot D^2}{32 \cdot \eta \cdot l}$$

$$v = 0.01822 \frac{m}{s}$$

Mathcad file for pressure calculation of balancing two menisci (section4.2):

$\gamma := 0.0728\frac{N}{m}$ $\quad d := 90\cdot 10^{-6}m$ $\quad b_2 := 250\cdot 10^{-6}m$ $\quad b_1 := \frac{b_2}{3}$ $\quad \alpha_{sa} := 36$ $\quad \alpha_{la} := 104$

$\alpha_{sr} := 24$ $\quad \alpha_{lr} := 77$

$$\Delta P_i := \gamma\cdot\left[\frac{(2\cdot d + b_1)\cdot\cos(\alpha_{sa}\cdot deg) + b_1\cdot\cos(\alpha_{la}\cdot deg)}{d\cdot b_1} - \frac{(2\cdot d + b_2)\cdot\cos(\alpha_{sr}\cdot deg) + b_2\cdot\cos(\alpha_{lr}\cdot deg)}{d\cdot b_2}\right]$$

$$\Delta P_{ii} := \gamma\cdot\left[\frac{\left[(2\cdot d + b_1)\cdot\cos(\alpha_{sr}\cdot deg) + b_1\cdot\cos(\alpha_{lr}\cdot deg)\right]}{d\cdot b_1} - \frac{\left[(2\cdot d + b_2)\cdot\cos(\alpha_{sa}\cdot deg) + b_2\cdot\cos(\alpha_{la}\cdot deg)\right]}{d\cdot b_2}\right]$$

$\Delta P_i = 419.265Pa$ $\quad \Delta P_{ii} = 1.587\times 10^3 Pa$

Mathcad file for volume calculations (section 4.2):

$$k_1 := \frac{28.24 + 27.81}{\left(2 \cdot 250 \cdot 10^{-6}\right)} \qquad k_2 := \frac{10.11 + 10.91 + 10.53}{250 \cdot 10^{-6}} \qquad k := \frac{k_1 + k_2}{2} \qquad k = 1.191 \times 10^{5}$$

$$d := 90\,10^{-6}\,m \qquad b_2 := 250 \cdot 10^{-6}\,m \qquad b_1 := \frac{b_2}{3} \qquad A_1 := b_1 \cdot d \qquad A_2 := b_2 \cdot d$$

$$x_1 := \begin{pmatrix} 80 \\ 32 \\ 9 \\ 8 \\ 65 \end{pmatrix} \qquad y_1 := \begin{pmatrix} 102 \\ 119 \\ 126 \\ 122 \\ 119 \end{pmatrix} \qquad V_1 := \frac{x_1}{k} \cdot A_1 + \frac{y_1}{k} \cdot A_2 \qquad V_1 \cdot m = \begin{pmatrix} 2.43 \times 10^{-11} \\ 2.449 \times 10^{-11} \\ 2.436 \times 10^{-11} \\ 2.354 \times 10^{-11} \\ 2.656 \times 10^{-11} \end{pmatrix} m^3$$

$$V_{1m} := \frac{\sum V_1 \cdot m}{5} \qquad V_{1m} = 2.5 \times 10^{-11}\,m^3$$

$$x_2 := \begin{pmatrix} 87 \\ 6 \\ 8 \\ 112 \\ 8 \\ 124 \end{pmatrix} \qquad y_2 := \begin{pmatrix} 107 \\ 136 \\ 136 \\ 92 \\ 133 \\ 94 \end{pmatrix} \qquad V_2 := \frac{x_2}{k} \cdot A_1 + \frac{y_2}{k} \cdot A_2 \qquad V_2 \cdot m = \begin{pmatrix} 2.568 \times 10^{-11} \\ 2.606 \times 10^{-11} \\ 2.619 \times 10^{-11} \\ 2.442 \times 10^{-11} \\ 2.562 \times 10^{-11} \\ 2.556 \times 10^{-11} \end{pmatrix} m^3$$

$$V_{2m} := \frac{\sum V_2 \cdot m}{6} \qquad V_{2m} = 2.6 \times 10^{-11}\,m^3$$

$$x_3 := \begin{pmatrix} 103 \\ 196 \\ 83 \\ 92 \\ 90 \\ 96 \\ 93 \\ 101 \\ 84 \end{pmatrix} \qquad y_3 := \begin{pmatrix} 122 \\ 125 \\ 133 \\ 123 \\ 129 \\ 127 \\ 125 \\ 120 \\ 128 \end{pmatrix} \qquad V_3 := \frac{x_3}{k} \cdot A_1 + \frac{y_3}{k} \cdot A_2 \qquad V_3 \cdot m = \begin{pmatrix} 2.952 \times 10^{-11} \\ 3.594 \times 10^{-11} \\ 3.034 \times 10^{-11} \\ 2.902 \times 10^{-11} \\ 3.003 \times 10^{-11} \\ 3.003 \times 10^{-11} \\ 2.946 \times 10^{-11} \\ 2.902 \times 10^{-11} \\ 2.946 \times 10^{-11} \end{pmatrix} m^3$$

$$V_{3m} := \frac{\sum V_3 \cdot m}{9} \qquad V_{3m} = 3 \times 10^{-11}\,m^3$$

$$x_4 := \begin{pmatrix} 96 \\ 8 \\ 8 \\ 130 \\ 126 \\ 7 \\ 7 \\ 126 \\ 120 \\ 0 \end{pmatrix} \qquad y_4 := \begin{pmatrix} 77 \\ 105 \\ 105 \\ 58 \\ 57 \\ 104 \\ 104 \\ 54 \\ 65 \\ 105 \end{pmatrix} \qquad V_4 := \frac{x_4}{k} \cdot A_1 + \frac{y_4}{k} \cdot A_2 \qquad V_4 \cdot m = \begin{pmatrix} 2.058 \cdot 10^{-11} \\ 2.033 \cdot 10^{-11} \\ 2.033 \cdot 10^{-11} \\ 1.914 \cdot 10^{-11} \\ 1.869 \cdot 10^{-11} \\ 2.008 \cdot 10^{-11} \\ 2.008 \cdot 10^{-11} \\ 1.813 \cdot 10^{-11} \\ 1.983 \cdot 10^{-11} \\ 1.983 \cdot 10^{-11} \end{pmatrix} m^3$$

$$V_{4m} := \frac{\sum V_4 \cdot m}{10} \qquad V_{4m} = 2 \times 10^{-11}\,m^3$$

Mathcad file for calculating flow times in y-direction (section 4.2):

$$k_1 := \frac{28.24 + 27.81}{\left(2 \cdot 250 \cdot 10^{-6}\right)} \quad k_2 := \frac{10.11 + 10.91 + 10.53}{250 \cdot 10^{-6}} \quad k := \frac{k_1 + k_2}{2} \quad \eta := 8.91 \cdot 10^{-4} \frac{N \cdot s}{m^2}$$

$$k_1 = 1.121 \times 10^5 \quad k_2 = 1.262 \times 10^5 \quad k = 1.191 \times 10^5 \quad \gamma := 0.0728 \frac{N}{m}$$

$$d := 9010^{-6} m \quad b_2 := 250 \cdot 10^{-6} m \quad b_1 := \frac{b_2}{3} \quad A_1 := b_1 \cdot d \quad A_2 := b_2 \cdot d$$

$$D_1 := \frac{4 \cdot A_1}{2b_1 + 2d} \quad D_2 := \frac{4 \cdot A_2}{2b_2 + 2d} \quad \alpha_{sa} := 36 \quad \alpha_{sr} := 24 \quad \alpha_{la} := 104 \quad \alpha_{lr} := 77$$

$$Py(p_a) := \gamma \cdot \left[\frac{(b_1 + 2d) \cdot \cos(\alpha_{sr} \cdot deg) + b_1 \cdot \cos(\alpha_{lr} \cdot deg)}{A_1} - \frac{(b_2 + 2d) \cdot \cos(\alpha_{sa} \cdot deg) + b_2 \cdot \cos(\alpha_{la} \cdot deg)}{A_2} \right] - p_a$$

$$P_{yi}(p_a) := \frac{Py(p_a)}{32 \cdot \eta} \quad K_1 := D_1^{-2} - D_2^{-2} A_1^{2} A_2^{-2} \quad K_2(V) := D_2^{-2} \cdot A_1 \cdot A_2^{-2} V$$

$$t_y(x, x_0, V, p_a) := \overrightarrow{\left[(2 \cdot P_{yi}(p_a))^{-1} \cdot \left[K_1 \cdot (x^2 - x_0^{2}) + \overrightarrow{[2 \cdot K_2(V) \cdot (x - x_0)]} \right] \right]}$$

$$v := \begin{pmatrix} 80 \\ 32 \\ 87 \\ 82 \\ 90 \\ 93 \\ 101 \\ 84 \\ 96 \\ 126 \\ 120 \end{pmatrix} \quad X_0 := \frac{v}{k} \quad T := \begin{pmatrix} 0.28 \\ 0.36 \\ 1.92 \\ 0.32 \\ 0.28 \\ 0.36 \\ 0.68 \\ 0.16 \\ 0.56 \\ 0.4 \\ 0.2 \end{pmatrix} \quad E := \begin{pmatrix} 32 \\ 9 \\ 6 \\ 18 \\ 17 \\ 17 \\ 0 \\ 0 \\ 8 \\ 7 \\ 0 \end{pmatrix} \quad X := \frac{E}{k} \quad P := \begin{pmatrix} 988 \\ 988 \\ 993 \\ 997 \\ 996 \\ 996 \\ 997 \\ 995 \\ 996 \\ 996 \\ 995 \end{pmatrix} \quad V_t := \begin{pmatrix} 2.5 \times 10^{-11} \\ 2.5 \times 10^{-11} \\ 2.6 \times 10^{-11} \\ 3.0 \times 10^{-11} \\ 3.0 \times 10^{-11} \\ 3.0 \times 10^{-11} \\ 3.0 \times 10^{-11} \\ 3.0 \times 10^{-11} \\ 2.0 \times 10^{-11} \\ 2.0 \times 10^{-11} \\ 2.0 \times 10^{-11} \end{pmatrix}$$

$$P_a := (1009 - P) \cdot 100 \cdot Pa$$

$$t_y(X \cdot m, X_0 \cdot m, V_t \cdot m^3, P_a) =$$

	0
0	1.812·10 -3
1	4.618·10 -4
2	0.108
3	-3.115·10 -3
4	-5.017·10 -3
5	-5.325·10 -3
6	-4.949·10 -3
7	-7.539·10 -3
8	-5.311·10 -3
9	-8.716·10 -3
10	-0.012

s

$T =$

	0
0	0.28
1	0.36
2	1.92
3	0.32
4	0.28
5	0.36
6	0.68
7	0.16
8	0.56
9	0.4
10	0.2

Mathcad file for calculating flow times in x-direction (section 4.2):

$$k_1 := \frac{28.24 + 27.81}{\left(2 \cdot 250 \cdot 10^{-6}\right)} \quad k_2 := \frac{10.11 + 10.91 + 10.53}{250 \cdot 10^{-6}} \quad k := \frac{k_1 + k_2}{2} \quad \eta := 8.91 \cdot 10^{-4} \frac{N \cdot s}{m^2}$$

$$k_1 = 1.121 \times 10^5 \quad k_2 = 1.262 \times 10^5 \quad k = 1.191 \times 10^5 \quad \gamma := 0.0728 \frac{N}{m}$$

$$d := 90 \cdot 10^{-6} m \quad b_2 := 250 \cdot 10^{-6} m \quad b_1 := \frac{b_2}{3} \quad A_1 := b_1 \cdot d \quad A_2 := b_2 \cdot d$$

$$D_1 := \frac{4 \cdot A_1}{2b_1 + 2d} \quad D_2 := \frac{4 \cdot A_2}{2b_2 + 2d} \quad \alpha_{sa} := 36 \quad \alpha_{sr} := 24 \quad \alpha_{la} := 104 \quad \alpha_{lr} := 7$$

$$P_x := \gamma \cdot \left[\frac{\left(b_1 + 2d\right) \cdot \cos\left(\alpha_{sa} \cdot deg\right) + b_1 \cdot \cos\left(\alpha_{la} \cdot deg\right)}{A_1} - \frac{\left(b_2 + 2d\right) \cdot \cos\left(\alpha_{sr} \cdot deg\right) + b_2 \cdot \cos\left(\alpha_{lr} \cdot deg\right)}{A_2} \right]$$

$$P_{xi} := \frac{P_x}{32 \cdot \eta} \quad K_1 := D_1^{-2} - D_2^{-2} A_1^{2} A_2^{-2} \quad K_2(V) := D_2^{-2} \cdot A_1 \cdot A_2^{-2} V$$

$$t_x\left(x, x_0, V\right) := \left(2 \cdot P_{xi}\right)^{-1} \cdot \left[K_1 \cdot \left(x^2 - x_0^{\,2}\right) + \overrightarrow{\left[2 \cdot K_2(V) \cdot \left(x - x_0\right)\right]} \right]$$

$$v := \begin{pmatrix} 8 \\ 8 \\ 8 \\ 33 \\ 3 \\ 0 \\ 0 \\ 0 \\ 8 \\ 7 \end{pmatrix} \quad X_0 := \frac{v}{k} \quad E := \begin{pmatrix} 65 \\ 112 \\ 124 \\ 103 \\ 96 \\ 92 \\ 96 \\ 81 \\ 130 \\ 126 \end{pmatrix} \quad X := \frac{E}{k} \quad V_t := \begin{pmatrix} 2.5 \times 10^{-11} \\ 2.6 \times 10^{-11} \\ 2.6 \times 10^{-11} \\ 2.9 \times 10^{-11} \\ 2.9 \times 10^{-11} \\ 2.9 \times 10^{-11} \\ 2.9 \times 10^{-11} \\ 2.9 \times 10^{-11} \\ 1.9 \times 10^{-11} \\ 1.9 \times 10^{-11} \end{pmatrix} \quad T := \begin{pmatrix} 0.04 \\ 0.04 \\ 0.04 \\ 0.12 \\ 0.04 \\ 0.06 \\ 0.04 \\ 0.04 \\ 0.08 \\ 0.08 \end{pmatrix}$$

$$t_x\left(X \cdot m, X_0 \cdot m, V_t \cdot m^3\right) =$$

	0
0	$2 \cdot 10^{-3}$
1	$5.1 \cdot 10^{-3}$
2	$6.1 \cdot 10^{-3}$
3	$3.9 \cdot 10^{-3}$
4	$4.1 \cdot 10^{-3}$
5	$3.9 \cdot 10^{-3}$
6	$4.2 \cdot 10^{-3}$
7	$3.1 \cdot 10^{-3}$
8	$6.2 \cdot 10^{-3}$
9	$5.9 \cdot 10^{-3}$

s

$T =$

	0
0	0.04
1	0.04
2	0.04
3	0.12
4	0.04
5	0.06
6	0.04
7	0.04
8	0.08
9	0.08